Available online at www.sciencedirect.com
SCIENCE DIRECT®
Journal of Petroleum Science and Engineering 39 (2003) 261–273
JOURNAL OF PETROLEUM SCIENCE & ENGINEERING
www.elsevier.com/locate/jpetscieng

Wettability and morphology of mica surfaces after exposure to crude oil

Jill S. Buckley*, David L. Lord

Petroleum Recovery Research Center, New Mexico Tech, Socorro, NM, USA

Received 12 March 2002; received in revised form 26 August 2002

Abstract

Reservoir wettability is determined by interactions between crude oil and mineral surfaces, mediated by an aqueous phase. Contact angles between immiscible fluids have long been used as probes to assess the effective wetting condition of surfaces after exposure to brine and oil, but there is a limit to the amount of information that can be deduced from contact angles in such nonideal conditions.

In this study, atomic force microscopy (AFM) has been used to observe mica surfaces treated with a series of crude oils that produce a wide range of wetting conditions—water-advancing contact angles on these surfaces vary from water-wet to oil-wet. In the most water-wet case, the only adsorbed features appear to be small, water-wet particles that are probably inorganic. All of the other oils deposited organic coatings, with varying thickness, morphology, and durability. Weakly water-wet systems exhibited many surface features, but the waitings tended to be unstable and to detach from the surface, especially during AFM scanning in water. The most oil-wet systems exhibited thick, stable organic coatings that were not disturbed by AFM scanning.

Keywords: AFM; Wettability; Adsorption; Crude oil

1. Introduction

Exposure to crude oil alters rock wettability as components from the oil adsorb or otherwise deposit onto exposed mineral surfaces. Pure hydrocarbons produce no such deposits; high energy surfaces exposed only to paraffinic or aromatic compounds remain water-wet. Crude oils, however, contain varying amounts of polar constituents, often referred to as resins and asphaltenes. Under the right circumstances, components from these fractions can adsorb and/or deposit, changing the effective wetting of the mineral surfaces (Buckley, 2001). The wetting conditions produced can vary depending on a number of key factors that include the compositions of oil, brine, and surface minerals, their spatial distribution, and thermodynamic variables (Anderson, 1986).

Measurements of the contact angles—advancing and receding—between a crude oil and brine on a clean, smooth surface have shown significant hysteresis and changes that continue over long periods of contact time (e.g., Treiber et al., 1972). Experimental difficulties include pinning of the three-phase contact line and development of rigid films at the oil/water

* Corresponding author. Petroleum Recovery Research Center, New Mexico Institute of Mining and Technology (NMIMT), 801 Leroy Place, Socorro, NM 87801-4796, USA. Tel.: +1-505-835-5405; fax: +1-505-835-6031.

E-mail address: jill@prrc.nmt.edu (J.S. Buckley).

0920-4105/03/$ - see front matter © 2003 Elsevier Science B.V. All rights reserved.
doi:10.1016/S0920-4105(03)00067-6

interface. Contact angles between probe fluids on surfaces after contact with crude oil have been used to demonstrate some of the interactions that can occur between crude oil components and mineral surfaces in the presence of an aqueous phase (Buckley et al., 1998) and the persistence of hysteresis between advancing and receding conditions (Xie et al., 2002).

Contact angles alone, however, cannot fully describe the resulting surfaces, which may be both physically and chemically heterogeneous. Some of the surface techniques that have been applied to investigate the material that remains on surfaces after exposure to crude oil or to crude oil fractions such as asphaltenes and resins include pyrolysis, Fourier transform infrared spectroscopy (FTIR), X-ray photoelectron spectroscopy (XPS), scanning electron microscopy (SEM), and atomic force microscopy (AFM). Only those studies that focus on interactions between crude oils and solids in the presence of an aqueous phase and that attempt to link their results to more usual measures of wetting (i.e., contact angles or imbibition-based tests in porous media) are reviewed here.

Wolcott et al. (1993) compared wettability as measured by the Amott test (Amott, 1959) with a pyrolysis technique that measures the amount of deposited material. Total organic carbon is subdivided into solvent extractable material, high molecular weight and/or polar compounds, and some oxygenated constituents. Changes in wettability were demonstrated with CO_2 flooding and exposure to KOH, but little correlation was found between the extent of wettability alteration and the amount of organic material deposited.

XPS can identify all atomic species heavier than He within the top 5 nm of a surface and it can differentiate on the basis of bond strength between organic and inorganic carbon. Such chemical detail holds the promise of identifying the species responsible for wetting alteration, but in practice, there are problems with surface contamination and its application is further limited by the necessity for high vacuum. It has been used in several studies to quantify the amount of organic carbon on rock surfaces and to relate adsorbed carbon to empirical measures of rock wettability such as the Amott and USBM tests (Mitchell et al., 1990; Quet et al., 1992; Toledo et al., 1996; Durand and Beccat, 1998). Imaging with XPS clearly differentiates between strongly oil-wet and strongly water-wet conditions and shows heterogeneity of mixed-wet rock slices (Hazell and Perry, 1998).

SEM has been used to produce images of rock surfaces and associated liquid phases. In cryo-SEM (Sutanto et al., 1990; Robin et al., 1995, 1999), fluids are frozen in place, the sample is coated and imaging takes place in a high vacuum. ESEM (Gauchet et al., 1993; Robin et al., 1999) is a technique that enables imaging in an environmental chamber rather than in a high vacuum. Energy dispersive X-ray spectrometry (EDS) can be used with either technique to identify fluids. Both show the proximity of fluids to specific minerals within the pore space, from which wettability is inferred. Films as thin as 0.1 μm can be imaged and identified, but the nanometer resolution that would be required to observe adsorbed layers of one or a few molecular diameters is not yet available.

AFM provides a force map that represents a combination of chemical and topological information at scales ranging from microns to angstroms. Force measurements between a crude oil drop and mica surface were reported by Basu and Sharma (1996). Their measurements of water film stability as a function of pH and salinity are in general agreement with adhesion tests (Buckley and Morrow, 1992). Imaging of oil-treated surfaces in air has been reported using both tapping mode (Buckley et al., 1997) and contact mode (Yang et al., 1999), but resolution of surface features was limited.

Questions remain about both the chemical nature and the physical distribution of organic material that is adsorbed or otherwise deposited on mineral surfaces when they are exposed to crude oils in the presence of an aqueous phase. To address these questions, an improved contact mode AFM technique has been developed (Lord and Buckley, 2002). In most AFM applications, the "height" of surface features is indicated by the distance that the sample surface must be moved by the feedback control system to maintain a constant deflection of the cantilever. On soft surfaces, however, the deflection signal produced by reducing the sensitivity of the feedback control system while monitoring the position of the cantilever can produce much more detailed images (Ducker and Grant, 1996). By utilizing a suite of techniques including minimizing the imaging force with a low spring-constant cantilever, reducing the influence of the feedback system, and using multiple imaging media (air, aqueous, and

nonaqueous fluids) information can be obtained about the organic material present on mineral surfaces, after exposure to crude oil, that has not been available from any other technique. Comparisons of the images obtained to contact angles between probe fluids on the same surfaces has shown that the extent of coverage and stability of the surface coating in water are both reflected in water–oil contact angles. There is unexpected diversity in the appearance of surface features resulting from exposure to different crude oils, even among surfaces that produce similar contact angles.

2. Experimental methods

2.1. Characterization of crude oils

Depressurized crude oil samples were obtained from a number of different sources. Lost Hills is a reservoir in California operated by Chevron. Mars is a platform in the Gulf of Mexico that produces from more than one reservoir; samples from two of these were provided by Shell. Tensleep oil is from Wyoming. The geographic origin of the remaining two samples was not specified. Tables 1–3 summarize chemical and physical properties of these six crude oil samples. Density (Mettler/Paar DMA 40), average molecular weight (measured by freezing point depression using a Cryoscope 5009 from Precision Systems), refractive indices (RI) (Index Instruments GPR11-37), and asphaltene characteristics are included in Table 1. The amount of asphaltene was measured by addition of an excess of *n*-heptane (ASTM D2007, 1980). The onset of asphaltene precipitation was induced by addition of *n*-heptane and was judged microscopically 1 day after mixing, as described by Wang and Buckley (2001). P_{RI} is the RI of the oil–heptane mixture with the least amount of heptane in which asphaltene aggregates are observed. Table 2 summarizes the acid (ASTM D664, 1989) and base numbers (ASTM D2896, 1998; Dubey and Doe, 1993); SARA analyses measured by an HPLC technique (Fan and Buckley, 2002) are given in Table 3.

Table 2
Acid and base numbers

Crude oil	Acid number (mg KOH/g oil)	Base number (mg KOH/g oil)	Base/acid
E-1XD-00	1.56	2.98	1.91
E-1XR-00	0.54	2.02	3.74
Lost Hills	1.90	6.05	3.18
Mars-Pink	3.92	2.30	0.53
Mars-Yellow	0.37	1.79	4.86
Tensleep	0.16	0.96	6.00

2.2. Treatment of mica surfaces

Thick water films can prevent adsorption of crude oil components on mineral surfaces (Buckley et al., 1998). The opposite extreme—exposing surfaces to oil in the absence of water—leads to wetting alteration, but with different wetting characteristics than are found when water is present. When water is present as a thin film, attractive electrostatic and van der Waals forces can combine to render the water film unstable, leading to adsorption of positively charged oil species on negatively charged surfaces. An aqueous phase with low salinity (less than ~ 0.1 M), no divalent or multivalent ions, and pH greater than 2

Table 1
Crude oil and asphaltene properties

Crude oil	°API	Density at 20 °C (g/cm^3)	Average MW	RI at 20 °C	*n*-C_7 P_{RI}	*n*-C_7 asphaltenes (%)
E-1XR-00	29.1	0.8781	218	1.4912	1.4071	0.27
E-1XD-00	22.3	0.9165	287	1.5141	1.4336	2.54
Lost Hills	22.6	0.9161	268	1.5137	1.4231	2.78
Mars-Pink	16.5	0.9524	309	1.5384	1.4288	4.77
Mars-Yellow	28.5	0.8804	258	1.4952	1.4261	1.86
Tensleep	31.2	0.8684	271	1.4877	1.4438	3.20

Table 3
SARA analyses

Crude oil	Saturates (%)	Aromatics (%)	Resins (%)	*n*-C_6 asphaltenes (%)
E-1XD-00	64.1	20.3	15.6	2.2
E-1XR-00	71.1	18.5	10.4	0.4
Lost Hills	50.0	22.5	24.2	3.4
Mars-Pink	35.3	32.4	26.4	6.0
Mars-Yellow	55.1	24.6	17.3	3.1
Tensleep	68.3	17.1	9.4	5.3

(near the zero point of charge of quartz and mica), but less than about 5 (the isoelectric points of many crude oils are in the range from less than 5 to about 7) maximizes the opportunity for water film instability, adsorption, and alteration of wettability.

2.2.1. Mica substrate

Muscovite mica was obtained from S&J Trading, Glen Oaks, NY. Disks for AFM tests (12.7 mm diameter) and rectangular samples for contact angle experiments (11 mm × 30 mm) were cut, cleaved to expose fresh surfaces, and immediately immersed in buffer solutions.

2.2.2. Buffer solutions

Buffers were prepared with ultrapure water, obtained by passing distilled, deionized water through Milli-Q cartridge filters (Millipore, Bedford, MA), and distilling once more in an all-glass system prior to use. Acidic brine was prepared by adding sodium acetate trihydrate ($NaC_2H_3O_2 \cdot 3H_2O$) (Fisher Scientific, Fair Lawn, NJ), acetic acid ($HC_2H_3O_2$), and sodium chloride (NaCl) in measured amounts to obtain a pH = 4.0, $[Na^+] = 0.01$ M solution. Basic brine was prepared by adding dibasic sodium phosphate 7-hydrate ($Na_2HPO_4 \cdot 7H_2O$) (J.T. Baker, Phillipsbug, NJ), monobasic sodium phosphate (NaH_2PO_4) (Aldrich Chemical, Milwaukee, WI), and NaCl in measured amounts to obtain a pH = 8.0, $[Na^+] = 1.0$ M solution.

2.2.3. Mica aging sequence in brine and oil

Mica samples were first immersed in buffers for at least 24 h, removed from brine, drained to remove bulk water, and transferred to oil without further drying. Samples were aged in oil for 14–21 days at room temperature and atmospheric pressure. After aging in oil, the mica was rinsed by dipping the sample in a toluene bath for about 1 s, removing the sample to allow the oil to drain off, and repeating the procedure until no visible oil adhered to the mica. Additional experimental details have been published previously (Lord and Buckley, 2002).

2.3. Oil/water contact angles on oil-treated surfaces

Contact angles were obtained on the oil-treated mica slides using decane and water as probe fluids by the captive drop method (Buckley et al., 1998), using a contact angle goniometer (Gaetner Scientific, Chicago, IL). A glass microburet was used to form and then withdraw a water droplet that pressed against a mica surface immersed in decane. The water advancing angle (θ_A) was measured with a newly expanded water drop, whereas the water receding angle (θ_R) was measured as the water drop was withdrawn. If the three-phase contact line pinned, the water receding angle was measured with a drop of decane expanding over a similarly treated mica surface immersed in water. Typically, a minimum of five different areas were tested on at least two mica samples. Contact angles measured through the water phase are reported.

2.4. AFM images of oil-treated surfaces

The microscope used for this work was a Nanoscope Multimode™ Atomic Force Microscope driven by a Nanoscope IIIa controller, software version 4.31r7 (Digital Instruments, Santa Barbara, CA). The AFM was equipped with a "fluid cell" (TappingMode Fluid Cell, Digital Instruments) designed to execute tapping mode and contact mode scans in air or liquids. Imaging for this study was conducted in contact mode with Olympus Oxide-Sharpened Silicon Nitride probes (Model OTR4, Digital Instruments). Both height signal and deflection signal images were captured. Height signal images were optimized by operating with high gain settings, while deflection signal images were optimized by imaging with low gain settings. The "E"-model scanner used in this work has a maximum horizontal scanning range of about 15 × 15 μm. The microscope was mounted on a vibration isolation table.

2.4.1. Surface roughness

The surface roughness of AFM samples can be quantified according to the mean roughness (R_a) calculation:

$$R_a = \frac{\sum_{i=1}^{N} \left| h_i - \bar{h} \right|}{N} \quad (1)$$

where h denotes elevation of the data point, and N is the number of points on the image. Any arbitrary rectangular area on an AFM image can be analyzed.

3. Results and discussion

3.1. Contact angles

Average contact angles are summarized in Table 4. Surfaces exposed to Mars-Pink are the most water-wet, those treated with E-1XD-00, Lost Hills, and Mars-Yellow oils remain weakly water-wet, while mica aged in the Tensleep and E-1XR-00 crudes are more oil wet. It should be noted that the values in Table 4 are averages of many measurements and that these measurements can be quite variable on these inherently heterogeneous surfaces; statistically identifiable outliers were removed from the data set.

The contact angles are summarized in Fig. 1a, using the water-advancing angles on surfaces first exposed to the pH 4 buffer as a basis for comparison. Other oil properties are also summarized in Fig. 1 including SARA fraction (Fig. 1b), the difference between RI_{oil} and P_{RI} (Fig. 1c), and acid/base properties (Fig. 1d). As shown in Fig. 1b, there is a general trend toward increasingly paraffinic composition with increasing values of θ_A. The amount of asphaltene is highest for Mars-Pink (lowest θ_A) and lowest for E-1XR-00 (highest θ_A); between these extremes, there is no correlation between amount of asphaltene and the contact angle results. The difference between RI of the oil (RI_{oil}) and the RI at the onset of asphaltene flocculation in response to addition of *n*-heptane (*n*-C_7 P_{RI}), shown in Fig. 1c, is an indication of asphaltene stability (Buckley et al., 1998). Higher values indicate more stable asphaltenes. Tensleep asphaltenes are noticeably less stable than the other five samples.

Table 4
Water/decane contact angles on oil-treated mica surfaces

Crude oil	Decane/water contact angles ± 1 S.D. (°)			
	Pretreatment brine: pH 4, I = 0.01 M		Pretreatment brine: pH 8, I = 1.0 M	
	θ_A	θ_R	θ_A	θ_R
E-1XD-00	51 ± 6	26 ± 6	45 ± 8	22 ± 2
E-1XR-00	137 ± 4	40 ± 4	55 ± 9	22 ± 2
Lost Hills	57 ± 10	23 ± 6	29 ± 16	10 ± 3
Mars-Pink	29 ± 5	10 ± 3	50 ± 13	23 ± 6
Mars-Yellow	62 ± 10	25 ± 6	31 ± 37*	8 ± 3
Tensleep	121 ± 8	68 ± 10	14 ± 3	12 ± 3

* This surface was too heterogeneous for meaningful values of the mean and standard deviation to be obtained.

Mars-Pink has the most stable asphaltenes in this group and is distinctive also in terms of its acid and base numbers (Fig. 1d) as the only oil with an acid number that exceeds its base number. Having more acids than bases reduces the likelihood of adsorption of positively charged organic bases on negatively charged mica surfaces. Among the other oils, there is an increasing trend in the ratio of base number to acid number up to a maximum of 6 for Tensleep. E-1XR-00, which has neither the highest base number to acid number ratio nor the least stable asphaltenes, does not appear to fit the trends established by the chemical properties of the other samples. Six is a very small number of oils on which to base any generalizations regarding the relationships between crude oil chemistry and wetting alteration.

3.2. AFM images

In parallel experiments, mica surfaces were imaged by AFM. Numerous regions were imaged on each mica sample to ensure that those selected for analysis and presentation were representative. The results are divided into different wetting regimes corresponding to the contact angle measurements reported in Table 4.

3.2.1. Water-wet mica surfaces

The most water-wet contact angles in Table 4 are for mica aged in {pH 8, 1 M} buffer and Tensleep crude oil. There was no evidence in the corresponding AFM image (Fig. 2) of any adsorbed or deposited organic material on the mica surface despite aging in Tensleep oil for 2 weeks, which is consistent with low values of both the water-advancing and water-receding contact angles. The mean surface roughness of the area indicated within the box in Fig. 2 is R_a = 0.05 nm, similar to R_a = 0.08 nm reported by Yang et al. (1999) for a clean mica surface.

In all the remaining examples, mica was first exposed to {pH 4, 0.01 M} aqueous buffer, then aged in various crude oils for at least 3 weeks. The *x*- and *y*-axis scales are always the same; to save space, only the *x*-axis scale is shown.

Mica aged in Mars-Pink is preferentially water-wet, as expected for this comparatively acidic oil. A stable film of water can exist between the oil and the acidic mica surface that prevents direct contact between the oil and mica (Buckley et al., 1998).

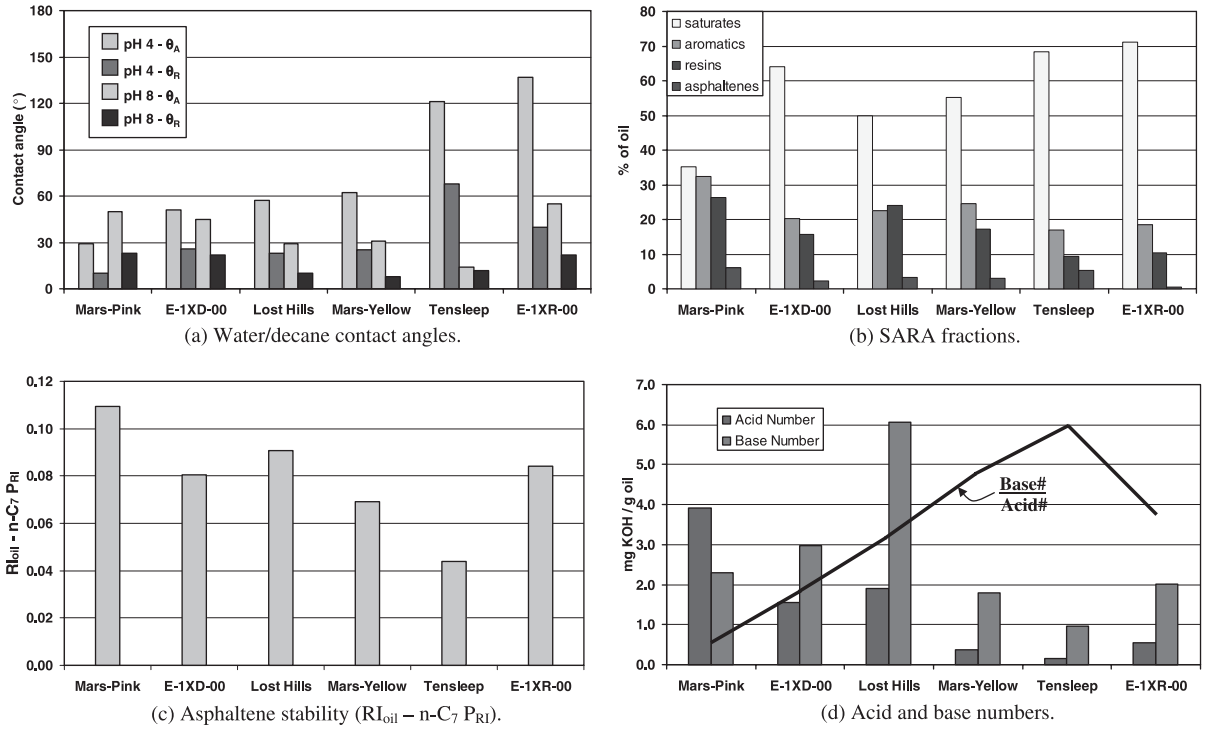

(a) Water/decane contact angles.

(b) SARA fractions.

(c) Asphaltene stability (RI_{oil} – n-C_7 P_{RI}).

(d) Acid and base numbers.

Fig. 1. Contact angles and chemical characteristics of selected crude oils.

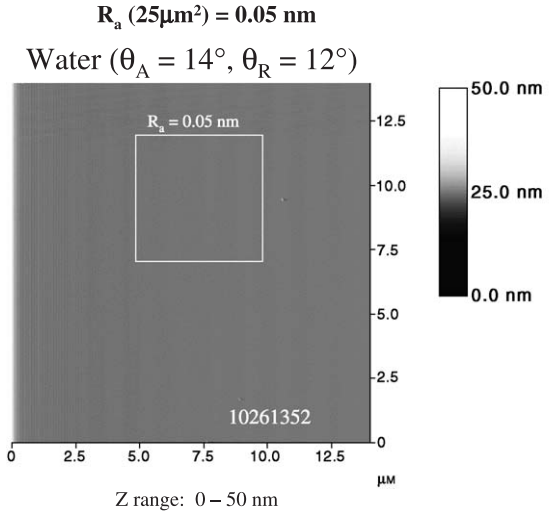

Fig. 2. AFM image of mica exposed first to {pH 8, 1 M} buffer then aged for 2 weeks in Tensleep crude oil. Height is indicated by a grayscale, with higher features appearing white (high Z values), and lower features black (low Z values). Since this surface is very smooth, it appears as a uniform shade of gray. (The grayscale bar is omitted from subsequent images; the bar shown here applies to other images with the Z range adjusted as indicated for each image.)

Fig. 3 shows three images of the surface in air, water, and decane, respectively. Examination of the surface in air shows a great deal of exposed mica ($R_a = 0.25 \pm 0.08$ nm) with circular areas of other material about 2 μm in diameter. In water, the 2-μm structures have disappeared, replaced by a dispersion of smaller (~ 0.2 μm) particles. Finally, when the water is removed and replaced by decane, roughly 2-μm-diameter structures appear dried on the surface. In the 3.5×3.5 μm^2 zoom shown in Fig. 3, it appears that the larger circular structures are made up of smaller particles, similar to those that dispersed across the surface in water. Thus it appears that the material left by Mars-Pink on the mica surface is a water-wet colloid that collects in the circular remnants left on the surface as water drops dry in air or in decane, but is dispersed when imaged under water. Roughness caused by the presence of this colloidal material is likely responsible for the increase in the water-advancing contact angles, although in the absence of organic deposits the system remains preferentially water-wet.

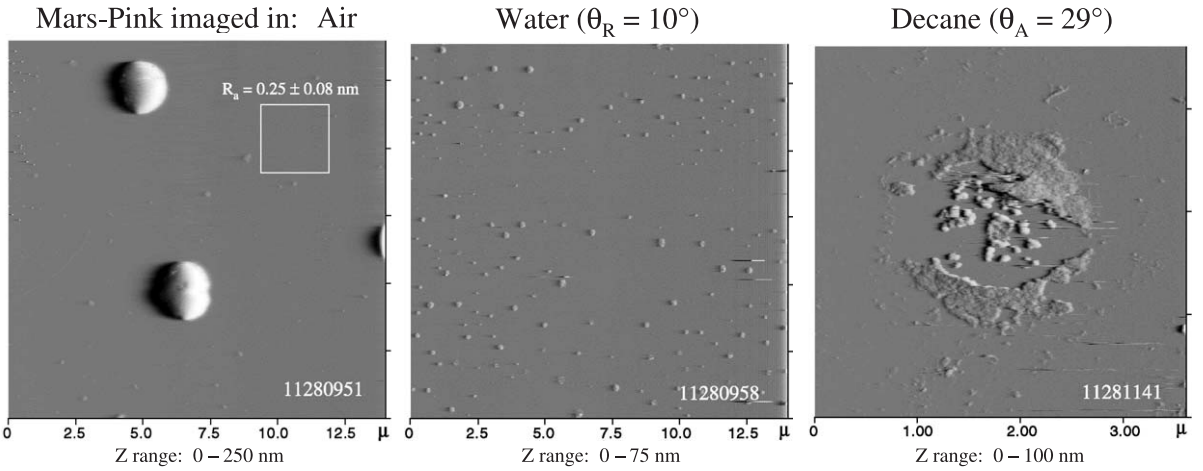

Fig. 3. AFM images of mica surfaces exposed to {pH 4, 0.01 M} buffer followed by aging in Mars-Pink crude oil. From left to right, images are shown that were obtained in air, water, and decane. Note that the decane image is at a different scale than the air and water images. For the image in air, R_a was measured for several rectangular areas away from the circular accumulations of material.

3.2.2. Weakly water-wet mica surfaces

Three oils (E-1XD-00, Lost Hills, and Mars-Yellow) produced surfaces on which average water-advancing angles were in the weakly water-wet range from 51° to 62°. Receding angles were also similar (23–26°). Although it might be expected that the AFM images of surfaces treated with these three oils would therefore be similar, they are in fact quite different from one another.

Mica aged in E-1XD-00 has a continuous coating that appears to be overlain by irregularly shaped submicron-sized particles (Fig. 4). Surface roughness of small areas between the irregularly shaped particles indicates that there is no bare mica ($R_a = 1.8 \pm 0.2$ nm in air; $R_a = 2.8 \pm 0.5$ nm under water; $R_a = 3.1 \pm 0.4$ nm under decane for areas of 0.4 μm^2). The fact that the appearance of the surface is almost identical in air, water, and decane suggests that in this case the imaged

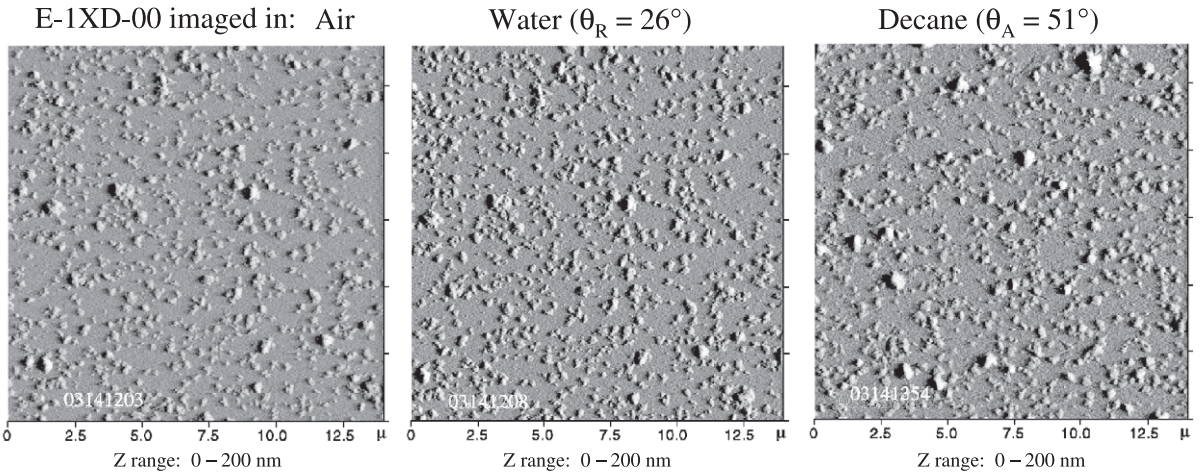

Fig. 4. AFM images of mica surfaces exposed to {pH 4, 0.01 M} buffer followed by aging in E-1XD-00 crude oil. From left to right, images are shown that were obtained in air, water, and decane.

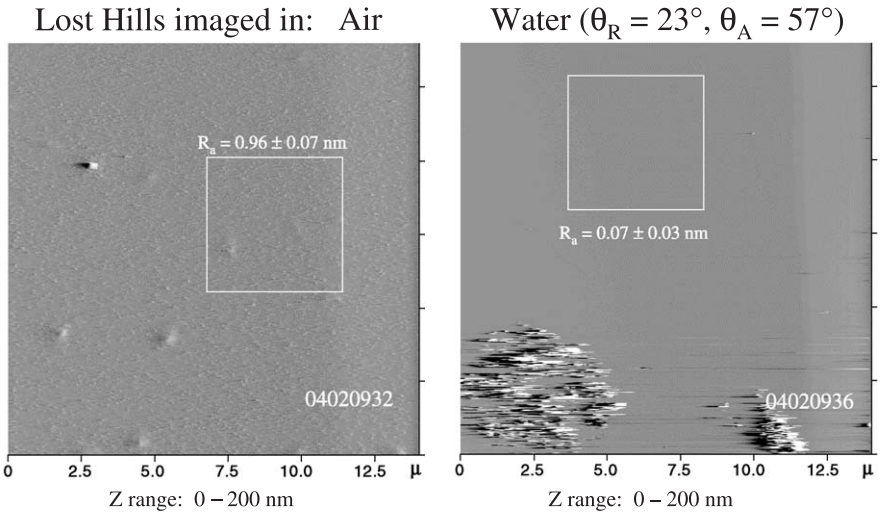

Fig. 5. AFM images of mica surfaces exposed to {pH 4, 0.01 M} buffer followed by aging in Lost Hills crude oil. The image on the left is in air; that on the right is in water.

features are topographical. Features with charged surfaces can also produce tip deflections, but their appearance would be different in water than in air and decane.

Lost Hills, shown in Fig. 5, exhibited an average advancing angle of $\theta_A = 57°$. Contact angle measurements were highly variable on this surface. Advancing angles that ranged from 28° to 86° suggest heterogeneity of coverage. Images in air were obtained, but under water most of the organic material was swept off the surface by the AFM tip during the first scan. Roughness measurements show that there is a layer of adsorbed material when the surface was imaged under air ($R_a = 0.96 \pm 0.07$ nm), but under water the surface appears to be mostly bare mica ($R_a = 0.07 \pm 0.03$ nm).

A great deal more material was left on mica surfaces aged in Mars-Yellow, as shown in Fig. 6. The difference in appearance between mica exposed

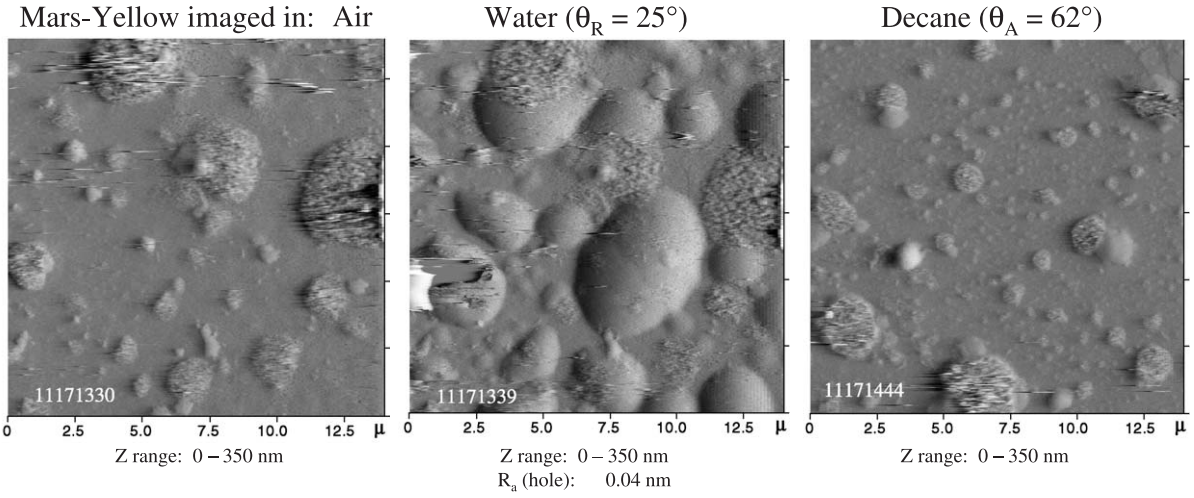

Fig. 6. AFM images of mica surfaces exposed to {pH 4, 0.01 M} buffer followed by aging in Mars-Yellow crude oil. From left to right, images are shown that were obtained in air, water, and decane.

to Lost Hills and that aged in Mars-Yellow is much greater than might be expected, given only a 5° difference in average advancing angles, which is not statistically significant. No bare mica is discernable under air. A relatively smooth coating is interspersed with rougher, approximately circular features. Why then is the surface not oil-wet? The image in water provides a clue. Under water, the nearly continuous coating appears to blister as though water is able to lift sections of the organic layer off the underlying mica. Note that the air and water images are of exactly the same area. A different area is shown under decane, but the features and appearance resemble those in air. The treated surface thus appears to be stable under decane and air, but not water.

3.2.3. Oil-wet mica surfaces

Higher contact angles were measured on mica surfaces aged in Tensleep oil. With an average θ_A of 121°, these surfaces are weakly oil-wet. The surface material was stable in all three imaging media (Fig. 7). Images of surfaces aged in Tensleep for varying amounts of time and in other solvents have been published previously (Lord and Buckley, 2002).

The most oil-wet surfaces were produced by aging in E-1XR-00. Images in air and decane were similar; adhesive interactions between the surface and tip precluded detailed imaging under water (Fig. 8). The coating on mica exposed to E-1XR-00 had fewer surface features than any of the other oil-treated surfaces examined in this study. Homogeneity of the organic coating may provide one explanation for the more oil-wet contact angles measured on this surface.

3.3. Thickness and durability of organic coatings

Although imaging forces are minimized, there is contact between the tip and organic surface. The result of that contact can vary dramatically, ranging from no apparent effect to cleaning of all organic material from the surface on the first or subsequent scans. These differences provide qualitative evidence about the strength of interactions between organic coating material and the inorganic surface as well as interactions laterally within the coating itself. The deposits from Lost Hills have strong interactions neither with the surface nor laterally within the organic layer and are scraped away under water (Fig. 5) by even the gentlest imaging force obtainable with the current instrument configuration. Alternatively, Mars-Yellow forms a coating with considerable lateral strength, but weak attachment to the surface is evidenced by blistering under water (Fig. 6). Estimates of coating thickness for the remaining oil-treated surfaces are summarized in Table 5. The coating produced by E-1XD-00 was stable during imaging, but could be scraped away by in-

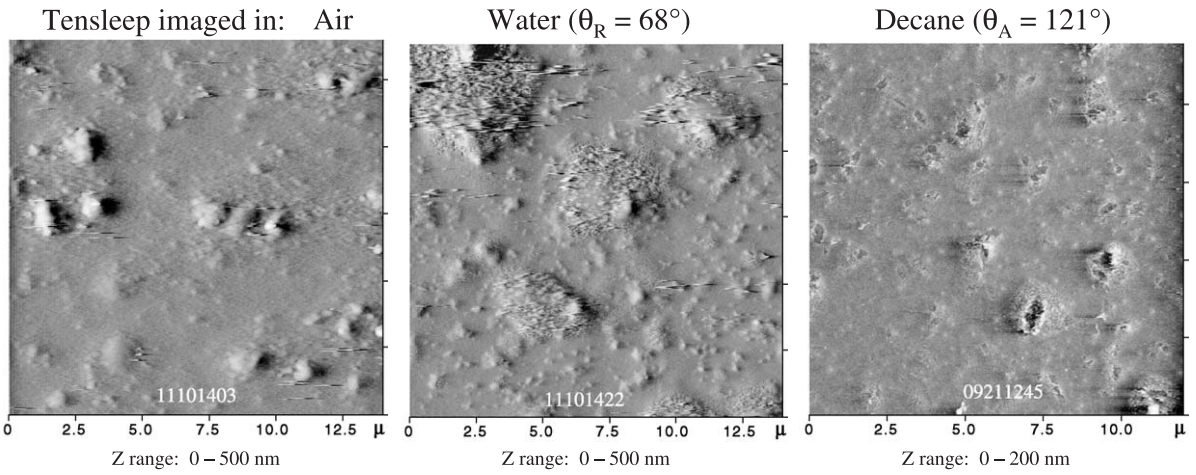

Fig. 7. AFM images of mica surfaces exposed to {pH 4, 0.01 M} buffer followed by aging in Tensleep crude oil. From left to right, images are shown that were obtained in air, water, and decane.

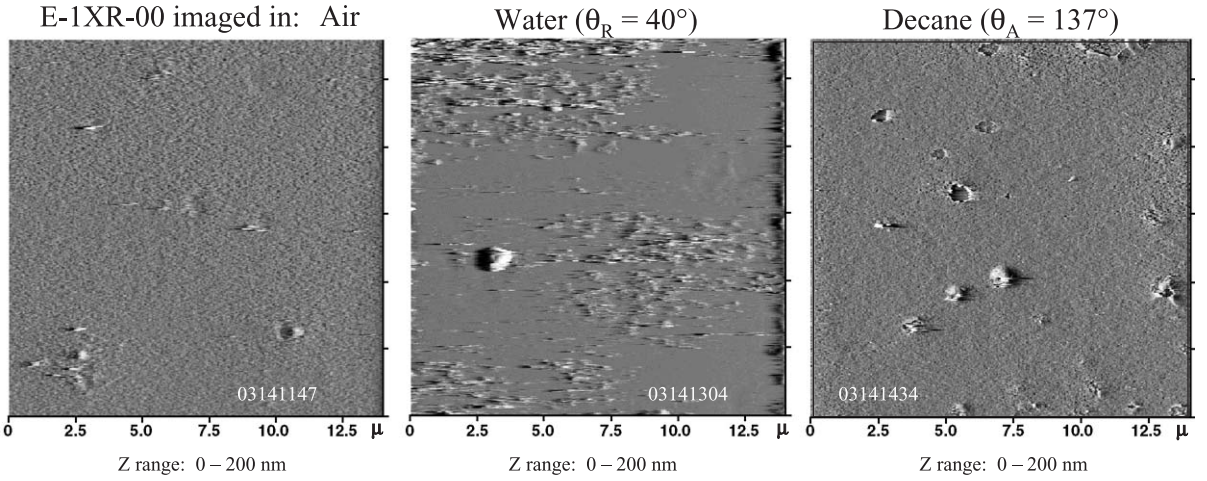

Fig. 8. AFM images of mica surfaces exposed to {pH 4, 0.01 M} buffer followed by aging in E-1XR-00 crude oil. From left to right, images are shown that were obtained in air, water, and decane.

creased imaging forces (Fig. 9). Tensleep treatments left a stable coating that could be scraped away by increased imaging forces coupled with addition of a good asphaltene solvent to the imaging medium (Fig. 10). The most oil-wet case, mica exposed to E-1XR-00, had a coating that maintained its integrity under both water and decane. Efforts to scrape a hole in this case were only partially successful, but an existing hole showed that the coating left by this oil is considerably thicker than that produced by any of the other oils (Fig. 11).

3.4. Organic deposits and wettability alteration

The AFM images provide confirmation of some of the conclusions drawn previously from contact angle studies. The ability of a stable water film to prevent any deposition, for example, is illustrated both by the small contact angles on surfaces exposed first to the {pH 8, 1 M} buffer, then to Tensleep crude oil and by the smooth mica surface in Fig. 2. Results are dramatically different for the same oil when the thin water film is not stable, as in the case where the buffer is {pH 4, 0.01 M} as shown in Fig. 7.

There is general correspondence between water advancing angles and the thickness and/or durability of the organic coatings. For the most water-wet case, Mars-Pink, no organic coating was detected. Among the weakly water-wet examples, E-1XD-00 produced an 11-nm-thick coating that could be readily removed by increasing the tip imaging force. What appeared to be a coating in air on mica exposed to Lost Hills was removed by even minimal imaging forces under water. Mars-Yellow produced a substantial coating, but it lifted off the mica surface under water. The main difference between Lost Hills and Mars-Yellow may be in the strength of lateral interactions among molecules within the coating that, in the case of Mars-Yellow, allow it to maintain its integrity even as it is being separated from the surface. Similar lateral interactions may also be responsible for the rigid films that are often observed at oil/water interfaces. Neither Lost Hills nor Mars-Yellow appeared to have established strong interactions with the mica surface, as both were displaced by water.

Table 5
Thickness of organic coatings on oil-treated mica surfaces

Crude oil	Coating thickness (nm)	Comments
Mars-Pink	not measurable	no coating detected
E-1XD-00	11	scraped area (Fig. 9)
Lost Hills	not measurable	coating disintegrates under water
Mars-Yellow	not measured	no appropriate height images available
Tensleep	14	scraped area (Fig. 10) (decane + amn, deflection image)
E-1XR-00	45	could not scrape clean, estimate from hole (Fig. 11)

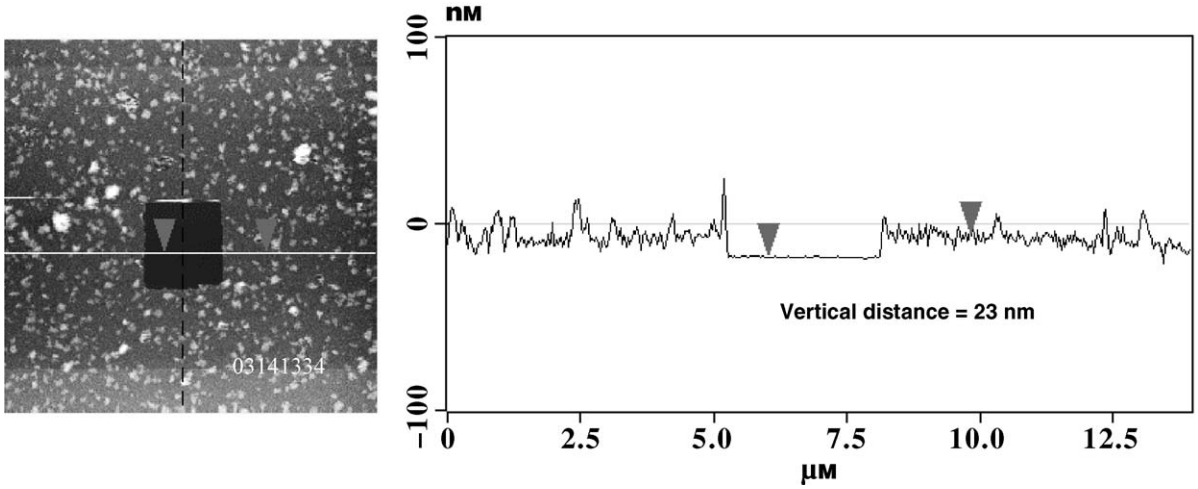

Fig. 9. This height image under decane shows that a hole could be scraped in the E-1XD-00 surface coating, revealing the smooth mica substrate beneath. The section view shown here depicts height signal (y-axis) versus distance along the section (x-axis).

The disparity among the images of surfaces with very similar contact angles is surprising. These observations help to explain why techniques such as XPS, which measure the amount of organic material on the surface, produce trends that are consistent with other measures of wettability, but with too much scatter in the results to be used to predict wetting directly from the analytical measurements. They also help to explain why Wolcott et al. (1993) saw little correspondence between the amount of material deposited and Amott wettability indices. The AFM images show that, in some cases, the amount of material may be dictated by film forming tendencies, but that these films are not necessarily strongly attached to surfaces. The rate of imbibition into weakly water-wet cores is often very slow during an initial induction period (Zhou et al., 2000). Surface coatings that separate slowly from the underlying mineral surfaces

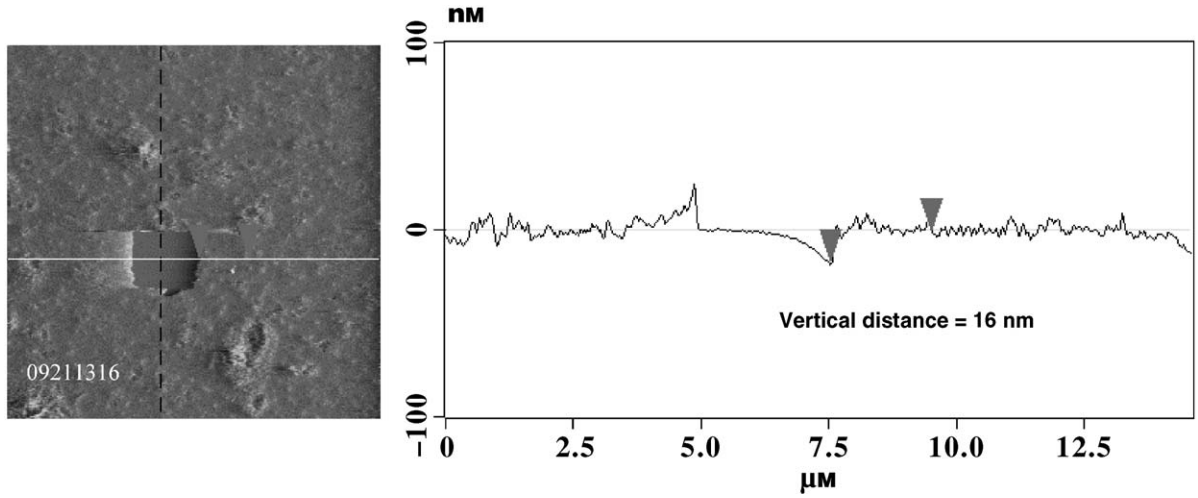

Fig. 10. A hole was scraped in the surface coating produced by aging in Tensleep when α-methyl naphthalene was added to the decane imaging medium. The scan direction is from right to left; an estimate of vertical distance must be made from the initial change in deflection of the tip as it enters the scraped area in this deflection image. (For additional discussion of the differences between deflection and height images, see Lord and Buckley, 2002.)

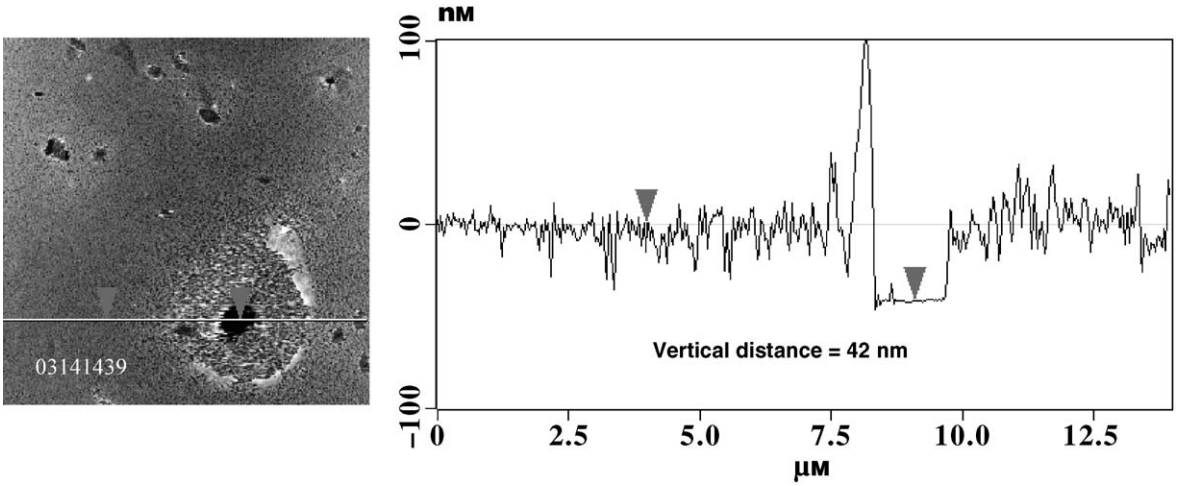

Fig. 11. The thickest coating was produced by aging mica in E-1XR-00 as shown in this height image under decane.

may be one factor contributing to the induction phenomenon.

The more oil-wet surfaces, Tensleep and E-1XR-00, both had thicker coatings that were resistant to removal by exposure to water or by mechanical disturbance. Coatings on mica exposed to Tensleep appeared to incorporate structures that, in another study (Lord and Buckley, 2002), were identified as flocculated asphaltenes. The coating was thick (14 nm) and resistant to water. Only after dilution of the imaging fluid with AMN, a good asphaltene solvent, could a hole exposing the mica surface be produced. E-1XR-00 produced the thickest, most resistant coating and the highest contact angles.

4. Conclusions

- In the presence of a stable water film, AFM images confirm that exposure to crude oil does not result in any perceptible organic deposition on mica surfaces.
- Water-advancing contact angles measured on surfaces exposed to a pH 4 buffer prior to aging in crude oil generally followed expected trends, with higher angles produced by more basic oils having less stable asphaltenes.
- Weakly water-wet surfaces had coatings that could readily be removed by increased imaging forces and by immersion in water.
- Coatings produced by exposure to Mars-Yellow had more lateral integrity than those deposited by Lost Hills crude oil. This difference was not reflected in contact angles, which were quite similar. The amount of material deposited by a crude oil may not be a good indicator of the extent of wetting alteration. The strength of interactions with the surface in the presence of water is an important factor.
- AFM images show that water-advancing angles are highest for oils that produce the thickest coatings that are resistant to disruption by the AFM tip. However, even apparently continuous organic coatings are not completely hydrophobic. Whether this is because the coatings are not as continuous as they appear or because the organic material is not completely hydrophobic is an important question that remains to be resolved.

Acknowledgements

This work was supported by the NETL of the US DOE through contract DE-AC26-99BC15204 and by support from industrial sponsors including BP, Chevron, Gaz de France, IFP, Norsk Hydro, and TotalFinaElf.

The authors are grateful to the Geochemistry Department at Sandia National Labs for providing access to their AFM for use in this study, to Shannon

Bays for contact angle measurements, and to Chevron, Shell, TFE, and Norman Morrow at the University of Wyoming for crude oil samples.

References

Amott, E., 1959. Observations relating to the wettability of porous rock. Trans. AIME 216, 156–162.

Anderson, W.G., 1986. Wettability literature survey: Part 1. Rock/oil/brine interactions and the effects of core handling on wettability. JPT 38, 1125–1144.

ASTM D664, 1989. Standard Test Method for Acid Number of Petroleum Products by Potentiometric Titration. ASTM, Philadelphia.

ASTM D2007, 1980. Standard Test Method for Characteristic Groups in Rubber Extender and Processing Oils by the Clay–Gel Adsorption Chromatographic Method. ASTM, Philadelphia.

ASTM D2896, 1998. Standard Test Method for Base Number of Petroleum Products by Potentiometric Perchloric Acid Titration. ASTM, Philadelphia.

Basu, S., Sharma, M.M., 1996. Defining the wettability state of mixed-wet reservoirs: measurement of critical capillary pressure for crude oils. SPE 36679, Proceedings of ATCE, Denver, 6–9 Oct.

Buckley, J.S., 2001. Effective wettability of minerals exposed to crude oil. Curr. Opin. Colloid Interface Sci. 6, 191–196.

Buckley, J.S., Morrow, N.R., 1992. An overview of crude oil adhesion phenomena. In: Toulhoat, H., Lecourtier, J. (Eds.), Physical Chemistry of Colloids and Interfaces in Oil Production. Éditions Technip, Paris, pp. 39–45.

Buckley, J.S., Liu, Y., Xie, X., Morrow, N.R., 1997. Asphaltenes and crude oil wetting—the effect of oil composition. SPEJ 2, 107–119.

Buckley, J.S., Liu, Y., Monsterleet, S., 1998. Mechanisms of wetting alteration by crude oils. SPEJ 3, 54–61.

Dubey, S.T., Doe, P.H., 1993. Base number and wetting properties of crude oils. SPERE 8, 195–200.

Ducker, W.A., Grant, L.M., 1996. Effect of hydrophobicity on surfactant surface-aggregate geometry. J. Phys. Chem. 100, 11507–11511.

Durand, C., Beccat, P., 1998. Use of XPS for reservoir sandstone wettability evaluation. Application to kaolinite and illite. J. Pet. Sci. Eng. 20, 259–265.

Fan, T., Buckley, J.S., 2002. Rapid and accurate SARA analysis of medium gravity crude oils. Energy and Fuels 16, 1571–1575.

Gauchet, R., Chenevier, P., Tricart, J.-P., 1993. Visualization of rock samples in their natural state using environmental scanning electron microscope. SPE 26620, Proceedings of ATCE, Houston, 3–6 Oct.

Hazell, L.B., Perry, D.L., 1998. Studies of the variation of surface composition within reservoir cores using imaging XPS and its relationship with wettability heterogeneity. Proceedings of the 5th International Symposium on Reservoir Wettability, Trondheim, 22–24 June.

Lord, D.L., Buckley, J.S., 2002. An AFM study of nanoscale features affecting at crude oil–water–mica interfaces. Colloids Surf., A 206, 531–546.

Mitchell, A.G., Hazell, L.B., Webb, K.J., 1990. Wettability determination: pore surface analysis. SPE 20505, Proceedings of ATCE, New Orleans, 23–26 Sept.

Quet, C., Chenevière, P., Glotin, G., Mourrel, M., 1992. Pore surface chemistry and wettability. In: Toulhoat, H., Lecourtier, J. (Eds.), Physical Chemistry of Colloids and Interfaces in Oil Production. Éditions Technip, Paris, pp. 81–88.

Robin, M., Rosenberg, E., Fassi-Fihri, O., 1995. Wettability studies at the pore level: a new approach by use of cryo-SEM. SPEFE 10, 11–19.

Robin, M., Combes, R., Rosenberg, E., 1999. Cryo-SEM and ESEM: new techniques to investigate phase interactions within reservoir rocks. SPE 56829, Proceedings of ATCE, Houston, 3–6 Oct.

Sutanto, E., Davis, H.T., Scriven, L.E., 1990. Liquid distributions in porous rock examined by cryo scanning electron microscopy. SPE 20518, Proceedings ATCE, New Orleans, 23–26 Sept.

Toledo, P.G., Araujo, Y.C., Leon, V., 1996. Wettability of oil-producing reservoir rocks as determined from X-ray photoelectron spectroscopy. J. Colloid Interface Sci. 183, 301–308.

Treiber, L.E., Archer, D.L., Owens, W.W., 1972. A laboratory evaluation of the wettability of fifty oil-producing reservoirs. SPEJ, 531–540.

Wang, J.X., Buckley, J.S., 2001. An experimental approach to prediction of asphaltene flocculation. SPE 64994, Proceedings OCS, Houston, 13–16 Feb.

Wolcott, J.M., Groves Jr., F.R., Trujillo, D.E., Lee, H.G., 1993. Investigation of crude-oil/mineral interactions: factors influencing wettability alteration. SPE Adv. Technol. Ser. 1, 117–126.

Xie, X., Morrow, N.R., Buckley, J.S., 2002. Contact angle hysteresis and the stability of wetting changes induced by adsorption from crude oil. Proc. 6th Internat. Symp. on Reservoir Wettability, Socorro, 27–28 Sept. Submitted to J. Pet. Sci. Eng. 33, 147–159.

Yang, S.-Y., Hirasaki, G.J., Basu, S., Vaidya, R., 1999. Mechanisms for contact angle hysteresis and advancing contact angles. J. Pet. Sci. Eng. 24, 63–73.

Zhou, X., Morrow, N.R., Ma, S., 2000. Interrelationship of wettability, initial water saturation, aging time, and oil recovery by spontaneous imbibition and waterflooding. SPEJ 5, 199–207.